RESEARCH ARTICLE

Porous polymer magnetic adsorbents for dye wastewater treatment

Tao Xue[1] · Feifei Shao[1] · Han Miao[1] · Xinxin Li[1]

Abstract

Dye wastewater discharged from industries has caused serious environmental problems. The recent decade has witnessed adsorption technology emerging as an advanced dye wastewater treatment method with great potential Therefore, we fabricated two kinds of magnetic porous adsorbents (HSF and HSVF) with different specific surface areas and activity sites. Both of which exhibit excellent performance with remarkable dye adsorption capacities, especially HSVF. We further investigated their adsorption kinetic and isotherm in detail. Therein, HSVF showed a nice desorption capacity, and it could be recycled rapidly by magnetism, which exhibited the advantages of effective, easy operation, and low cost. In addition, their adsorption kinetic and isotherm were further studied and compared in detail. The results revealed that introducing strong active sites could improve both the adsorption capacity and rate effectively even though sacrificing part of specific surface areas, indicating that active sites might play a dominant role during the dye adsorption process.

Introduction

Nowadays, water pollution has attracted great attention worldwide due to the high toxicity (Karaouzas et al. 2021; Nakamura 2010, 430; Xie et al. 2020), and the booming variety of contaminants with the development of industry, such as spilling oil, (Jin et al. 2019), organic pesticides (Bolukbasi et al. 2022; Kadirsoy et al. 2020, 6524; Yola 2022), antibiotics (Zhang et al. 2019, 39), and dyes (Yadav et al. 2021). Aiming at treating these contaminants, the development of detection (Kıran et al. 2019, H495; Pelin Böke et al. 2020, 105012; Karaman et al. 2021, 11222), separation (Naushad et al. 2019, 112075; Md. Munjur et al. 2020, 114356; Salman et al. 2023b, 157008), and degradation (Rajendran et al. 2022) methods is in urgent need. Among these contaminants, organic dye wastewater discharged from the textile and food industry has led to serious health and environmental crisis (Lv et al. 2019; Zhang et al. 2020). In order to separate dye-polluted wastewater efficiently, lots of separation technologies have been developed, including membrane separation, chemical flocculation, and adsorption (Cheng et al. 2018, 258; Pavithra et al. 2019, 1; Verma et al. 2012; Wu et al. 2022), among which the adsorption technologies have become very popular due to their low-cost, convenient, and easy operation (Islam et al. 2021, 105849).

The adsorbent is the core of adsorption technology. Different compositions and structures of adsorbents could generate different interactions with dye during the adsorption process, such as Van der Waals' force, electrostatic interaction, and $\pi-\pi$ interaction (Teo et al. 2022, 130039), thus impacting the adsorption performance. In general, porous structure and activity sites of adsorbents are considered the critical structural and compositional properties that have a great influence on adsorption behavior (Castaldo et al. 2021, 129463). Therefore, many inorganic porous materials were chosen because of their intrinsic high specific surface areas and designable pore structure (Cheng et al. 2011; Zhu et al. 2016, 239; El-Safty et al. 2011). Due to the lacking of activity sites, organic functionalization for inorganic materials were attempted to remove dye (Naushad et al. 2019, 112075). In recent years, organic porous materials were drawn to attention

✉ Xinxin Li
xinxinli@ecust.edu.cn

Han Miao
hmiao@ecust.edu.cn

1 Key Laboratory of Specially Functional Polymeric Materials and Related Technology (Ministry of Education), School of Materials Science and Engineering, East China University of Science and Technology, 130, Meilong Road, Shanghai 200237, People's Republic of China

in the adsorption field (Su et al. 2019, 17267; Wu et al. 2021; Xu et al. 2022; Zhang et al. 2021; Zhao et al. 2020, 123591). Hypercrosslinked polystyrene (HCP) was the most common organic porous material and received much attention in the adsorption field due to its remarkable structure and functional designability (Waheed et al. 2021). Recently, HCP with different structures was prepared, such as core-shell, yolk-shell (Zhou et al. 2019, 2924), and polymer brush (Guojun Xie et al. 2018, 8624). These structures with different specific surface areas displayed different adsorption performances further. In addition to the influence of specific surface areas on adsorption, another key factor is how the active sites affect adsorption performance. Introducing active sites could generate different interactions between adsorbents and adsorbates. Styrene had a robust copolymerization ability so that HCP could be modified by diverse functional monomers (Jiang and Huang 2016; Li et al. 2017, 109; Shi et al. 2020). The previous researches have proved that high specific surface areas and strong interactions were beneficial for improving adsorption performance. However, in most cases, high specific surface areas and strong active sites were not available simultaneously for HCP because the functional modification often results in the decrease of the specific surface areas (Castaldo et al. 2021, 129463; Zhao et al. 2020, 123591). Therefore, it is necessary for designing adsorbents to discuss the influence degree of specific surface areas and active sites on adsorption performance. In addition to the adsorption performance, secondary pollution of adsorbents was another noteworthy challenge for adsorption technology. So, lots of natural polymeric adsorbents were developed, such as chitosan (Salman et al. 2023b, 157008), rice flour, graham flour (Md. Munjur et al. 2020, 114356; Kubra et al. 2021b, 115541), turmeric powder (Kubra et al. 2021a, 115468), and wheat flour (Hasan et al. 2021, 114587); these materials were innocuous and biodegradable (Yeamin et al. 2021, 125920). Besides, collecting adsorbents from the water was another key factor to reduce secondary pollution. Designing magnetic adsorbents could be an effective and facile method to collect adsorbents fleetly for further processing (Chen et al. 2020; Essandoh et al. 2020; Zhang et al. 2013). Therefore, combining the great designability of HCP and magnetic Fe_3O_4, the porous polymer magnetic adsorbents not only had a nice adsorption performance but also could be recycled easily when compared to other composite materials.

Herein, two kinds of magnetic porous Fe_3O_4/HCP hybrid microparticles (HSF and HSVF) with different specific surface areas and active sites were obtained by mature mini-emulsion polymerization and Friedel-Crafts reaction. After that, sunset yellow (SY) which may cause lots of health crises was regarded as a model dye (Coros et al. 2020) to explore their different adsorption performances and mechanisms affected by specific surface areas and active sites. The result revealed that both adsorption rates and capacity could

be improved observably after introducing 10% of the molar fraction of strong positive active sites even though about 30% of specific surface areas were sacrificed. So, it could be concluded that active sites played a dominant role during the dye adsorption process. Meanwhile, the adsorbent could be recycled by magnetism, which certified that it was an effective method to reduce secondary pollution.

Materials and methods

Materials

Styrene (St), 4-vinylpyridine (4VP), divinylbenzene (DVB), sodium dodecyl sulfate (SDS), anhydrous ferric chloride ($FeCl_3$), ferrous sulfate heptahydrate ($FeSO_4 \bullet 7H_2O$), rhodamine B (RhB), and methyl blue (MB) were purchased from Aladdin Biochemistry Co. Ltd. St, 4VP, and DVB were filtered through the alkaline alumina column to remove the inhibitor for further use. Potassium persulfate (KPS) was purchased from Meryer Co. Ltd. and was recrystallized from water. 1,2-dichloroethane (DCE), ammonia ($NH_3 \bullet H_2O$), oleic acid (OA), dimethoxymethane (FDA), and N-hexadecane (HD) were purchased from Macklin Co. Ltd., and DCE was dried over CaH_2 and distilled before use. Sunset yellow (SY) was purchased from Beijing Warwick Chemical Co. Ltd. Except for the indication, other reagents were used without further purification.

Synthesis of porous adsorbent

Firstly, the OA-coated Fe_3O_4 (OA-Fe_3O_4) nanoparticle was synthesized by a facile coprecipitation method (the details were given in the supporting information). Then the hybrid microparticle was prepared through mini-emulsion polymerization. OA-Fe_3O_4 (1.5 g) was separated from water by the magnet and redispersed into a mixture of St (5 g, 48.1 mmol), DVB (0.5 g), and HD (0.15 g) under ultrasonication as the oil phase of the following mini-emulsion polymerization. SDS (0.25 g) was dissolved in water (50 mL) as the water phase. Then the oil phase was added dropwise to the water phase under mechanical stirring (500 rpm) for 30 min to form a raw emulsion. After that, the system was homogenized by ultrasonication under ice-cooling for 20 min at 225 W. The obtained emulsion was heated to 70°C, and KPS (0.05 g) was dissolved in 10 mL water and then joined to initiate the reaction. After 24 h, the hybrid microparticle (named SF) was collected by centrifugation at 8000 rpm for 15 min. For the functional microparticle (named SVF), 0.5 g of St (4.81 mmol) was replaced with 0.5 g of 4VP (4.76 mmol), and then the same reaction was conducted. The target product, Fe_3O_4-incorporated magnetic microparticles, could be collected and purified by magnetism; thus, the

polymeric by-product, microparticles without Fe_3O_4, could be removed conveniently.

The hypercrosslinked network was conducted by referring to the previous literature (Li et al. 2013; Li et al. 2016). The details were as the following: SF or SVF (0.5 g) was dispersed in DCE (20 mL) for 5 h to swell adequately under N_2 atmosphere, and then FDA (2 mL) and $FeCl_3$ (3.65 g) were added into the mixture at 45°C for 5 h. Next, the Friedel-Crafts reaction was heated at 80°C for 19 h. The resulting porous adsorbent was filtered and washed with methanol. After being washed in a Soxhlet with methanol for 24 h, the adsorbent was dried in a vacuum oven at 60°C for 24 h. The obtained materials are denoted as HSF and HSVF, and the preparation procedures and the schematic structure of adsorbents are illustrated in the supporting information Scheme S1.

Characterization

The structure data of Fe_3O_4 was recorded by X-ray diffraction (XRD, D/max2550VB/PC). Fourier transform infrared (FT-IR) spectra were investigated by a Nicolet FTIR 5700 spectrometer. The morphology of the hybrid microparticle was observed by transmission electron microscope (TEM, JEOL JEM-2100). Hydrodynamic diameter (D_h) obtained via dynamic light scattering (DLS) and zeta potential of adsorbents were measured on Malvern Zetasizer Nano ZS90. The specific surface area and porous structure of adsorbents were measured by nitrogen adsorption-desorption analysis (Micromeritics ASAP2460). The chemical composition of the SY and adsorbents after adsorption was obtained by X-ray photoelectron spectroscopy (Thermo Scientific ESCALAB 250Xi).

Batch adsorption experiments

The batch adsorption experiments were conducted in a constant temperature rocker rotator at different concentrations, times, temperatures, pH, and the solid-to-liquid ratios. The concentrations of the dye solutions after adsorption were determined by UV-vis spectrophotometer (UV-2450/2550, Shimadzu). Then the adsorption capacity was calculated by the following equations:

$$q_t = \frac{(C_0 - C_t) \times V}{m} \qquad (1)$$

$$q_e = \frac{(C_0 - C_e) \times V}{m} \qquad (2)$$

$$RE = \frac{C_0 - C_e}{C_0} \times 100\% \qquad (3)$$

$$q_d = \frac{C_d \times V}{m} \qquad (4)$$

$$DE = \frac{q_d}{q_e} \times 100\% \qquad (5)$$

$$q_r = q_e - q_d \qquad (6)$$

where C_0 (mg/L), C_t (mg/L), C_e (mg/L), and C_d (mg/L) were the initial, time t, equilibrium, and desorption concentrations of SY solutions, respectively. q_t (mg/g) and q_e (mg/g) represent the adsorption capacity at time t and equilibrium. V and m were the volume of dye solution and mass of adsorbent. RE (%) was the dye removal efficiency. q_d (mg/g) was the desorption capacity of each recycle. DE (%) represents the desorption efficiency, and q_r (mg/g) was the residual adsorption capacity after desorption each time.

Adsorption selectivity experiments were conducted at 298 K, pH = 2, and the mixing dye solutions were prepared by mixing the same volume of 200 mg/L of a single dye solution.

According to the batch adsorption experiments, the adsorption kinetics, isotherms, and adsorption mechanisms were investigated further.

Results and discussion

Synthesis and characterization of adsorbents

The Fe_3O_4 nanoparticle was prepared and modified by OA successfully (Figure S1). As for the hybrid microparticle, obvious cladding structures have appeared (Fig. 1a, b and Figure S2), and the hydrodynamic diameter of the hybrid microparticle was about 78.8 nm measured by DLS. Furthermore, according to the FT-IR spectrogram (Fig. 1c), the peaks at 2923 cm^{-1} and 3024 cm^{-1} were from stretching vibration of saturated and unsaturated C-H respectively, which demonstrated the successful preparation of SF. Besides, the characteristic peak at 1412 cm^{-1} was observed on the curve of SVF on account of the stretching vibration of the C=N bond from the pyridine ring.

The zeta potentials of these two adsorbents were researched (Fig. 1d). The general trend of the potentials of both HSF and HSVF decreased with the increase of pH values. The zeta potentials were positive at low pH and dropped to negative at higher pH values. When pH = 2, H^+ was adsorbed on the surface of HSF easily in such strong acid aqueous; therefore, HSF showed a positive value (8.12 mV). With the increase in pH value, the concentration of H^+ decreased, and when the aqueous solution became basic, the surface of HSF was occupied
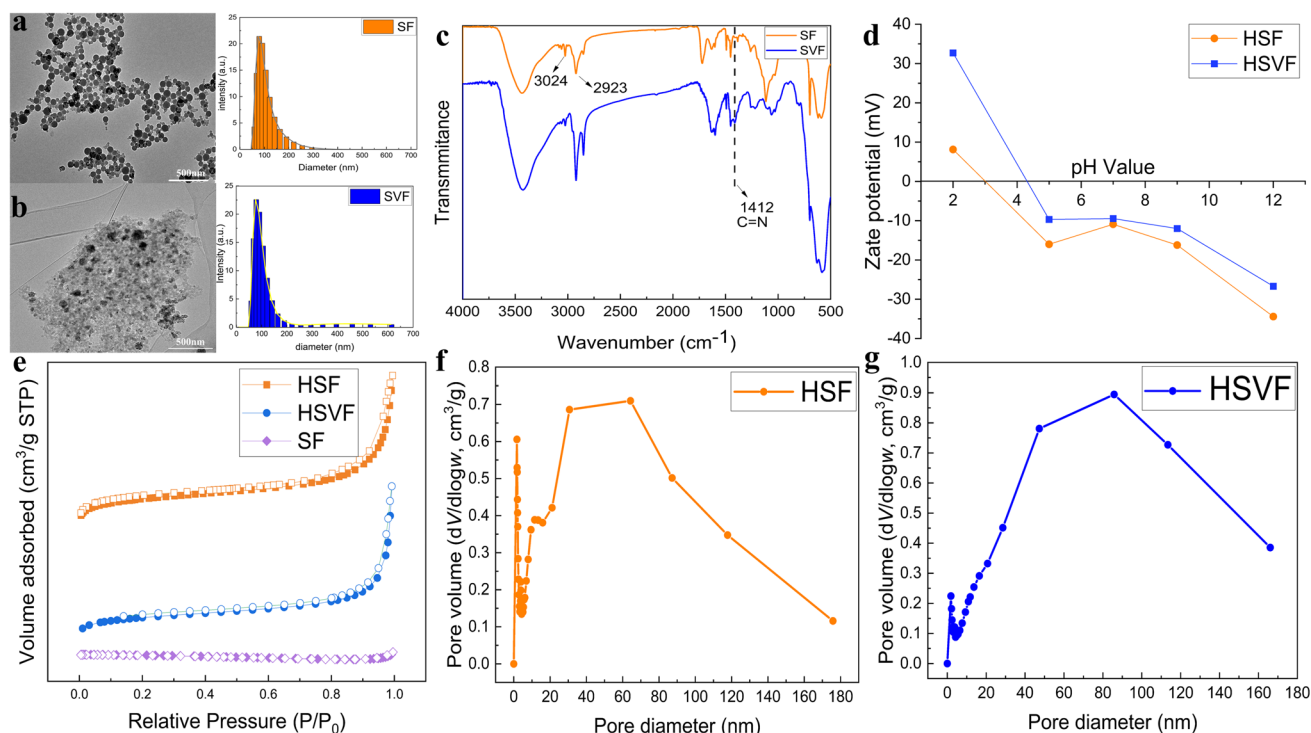
Fig. 1 **a**, **b** TEM images and hydrodynamic diameter (measured by DLS) of **a** SF and **b** SVF, **c** the FT-IR spectra of SF and SVF, **d** zeta potentials of HSF and HSVF, N$_2$ adsorption and desorption curves of SF, HSF, and HSVF, **f**, **g** the pore size curves of **f** HSF and **g** HSVF

by more OH$^-$, resulting in its potential decrease. As for HSVF, in addition to the adsorption of H$^+$ on the surface, its pyridine structure could be protonated, leading to a much higher positive potential than that of HSF at pH = 2. This also resulted in the higher potential values of HSVF than that of HSF at each pH across the entire pH range. When the pH value increased, deprotonation of the pyridine ring also contributed to the decrease of the potential.

For adsorbents, their specific surface area and porous structure were studied by N$_2$ adsorption-desorption analysis (Fig. 1e). From the curves, before hypercrosslinking, SF did not present the capacity of N$_2$ adsorption, while HSF had rapid N$_2$ adsorption at low relative pressure which demonstrated the existence of micropores in HSF. Furthermore, obvious hysteresis loops appeared on the curves of HSVF, but the hysteresis loops of HSF were almost suppressed revealing that adsorbent HSVF had a more mesoporous structure. According to Fig. 1f and g, the pores in HSF were micropores mainly, but there were more mesopores and macropores in HSVF so its specific surface area decreased by about 30% compared with that of HSF after substituting 10% molar fraction of St with 4VP.

When part of St was replaced by 4VP, the reactive sites were reduced for Friedel-Crafts reaction due to the strong polarity of the pyridine rings. In addition, the introduction of the pyridine rings to the molecular chain resulted in the

increase of the distance between the benzene rings, so it was more difficult for HSVF to form micropores than HSF. The detailed information about the specific surface areas is listed in Table 1.

Adsorption behavior of HSF and HSVF

The whole adsorption process is present in Fig. 2a. On account of the existence of Fe$_3$O$_4$, the extra merits clearly that the adsorbent could be facilely recycled by magnetic separation to avoid secondary pollution. There were lots of factors to affect the adsorption behavior of adsorbents. Firstly, pH had great influences on the existence of forms of contaminants (Hasan et al. 2023c, 134795) or adsorbents (Liu et al. 2021) and then affected the adsorption behaviors. Figure 2b indicates that the adsorption capacity of these two

Table 1 Summary of the specific surface area of HSVF and HSF

Adsorbent	S_{BET}[a] m^2/g	Sm[b] m^2/g	PV[c] cm^3/g
HSF	685.95	343.43	1.0058
HSVF	471.88	201.42	0.4593

[a]BET specific surface area of adsorbents; [b]t-plot micropore area of adsorbents; [c]pore volume calculated from the nitrogen isotherm
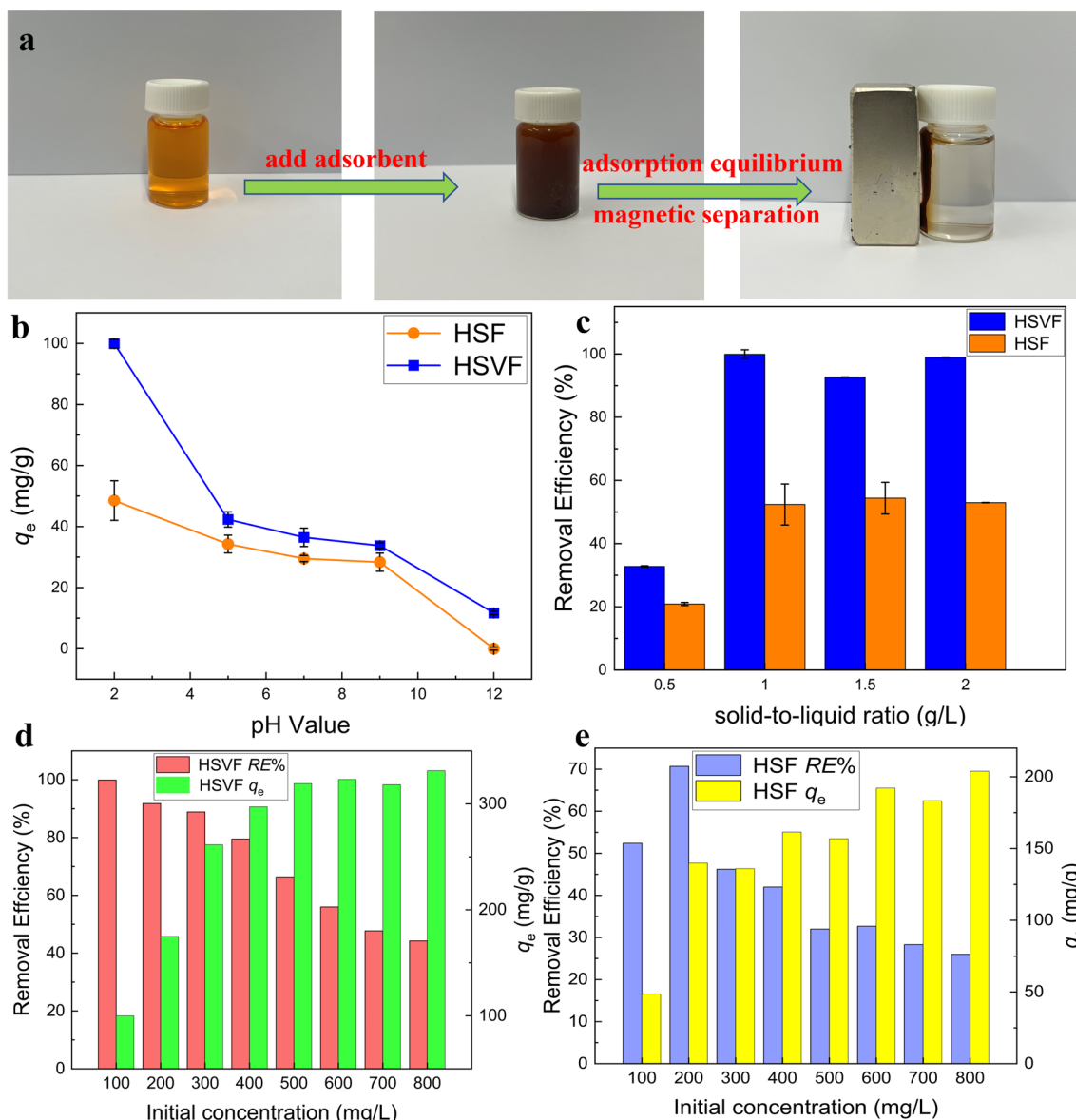
Fig. 2 **a** Photographs of adsorption and magnetic separation processes, **b** the influence of pH on adsorption capacity q_e, **e** the influence of solid-to-liquid ratios on removal efficiencies at 100 mg/L, **d**, **e** the influence of dye solution initial concentration on **c** HSVF and **d** HSF adsorption capacity q_e and removal efficiency RE

adsorbents was reduced by the increase in pH values. This was because SY was a kind of anionic dye stabilizing in an acid solution (its composition and structure are illustrated in Figure S3), its negative potential would make it diffuse into adsorbents easier because of the positive surface potential of adsorbents in the strong acid environment. What's more, the pyridine structure in HSVF could be protonated and produce strong electrostatic attraction with the sulfonate of SY molecule, making the incorporation stabler. With the increase in pH, the nanoparticle surface potential transformed from positive to negative; thus, electrostatic-interaction-caused dye diffusion would be limited by the resulting electrostatic

repulsion, and then the diffusion depended only on concentration gradient.

The solid-to-liquid was another important condition for the removal operation. From Fig. 2e, the removal efficiencies of HSVF and HSF reached the maximum when the ratio was 1 g/L, increasing the ratio would even make the efficiencies descend slightly. As for HSVF, nearly all of the dye molecule was adsorbed at 1 g/L, increasing the ratio might lead adsorbents to agglomerate because of the hydrophobicity, a corresponding increase in the diffusion path length further (Zou et al. 2013, 111). And the similar tendency occurred for HSF even though it did not reach saturation at 1g/L; it might

be caused by the low concentration gradient apart from the hydrophobicity.

Furthermore, the effect of initial concentration on dye adsorption was studied (Fig. 2d and e). For both of them, their adsorption capacity (q_e) enhanced with the increase in dye initial concentration and reached equilibrium at last. This could be explained that with the increase of initial concentration, a higher concentration gradient was generated, and dye molecules could diffuse into the pores of the adsorbent easier; therefore, the probability of adsorption was higher, and the q_e could be improved. However, when all the adsorption sites were occupied entirely by dye molecules, the adsorption capacity reached equilibrium. As for HSF, its removal efficiencies for SY solution decreased with the increase of initial concentration because of a disproportionate increase in the SY concentration versus the adsorbed SY molecules. When concentration rose from 500 to 800 mg/L, adsorption capacity almost achieve equilibrium, increasing concentration constantly result in a decline in the removal efficiency (Tang et al. 2021). Noticeably, the removal efficiency of HSF toward SY increased as the initial dye concentration rose from 100 to 200 mg/L and then decreased at a higher initial concentration. It could be stated that the HSF relied on concentration gradient more compared with HSVF; when the initial dye concentration rose to 200 mg/L,

its adsorption capacity increased greatly so that its removal efficiency had an obvious increment.

To further confirm the electrostatic attraction between HSVF and SY, the two kinds of adsorbents after adsorption at pH = 2 were characterized by XPS. As shown in Fig. 3b, the N 1S peak belonging to the azo structure of SY molecular was at 400.2eV; it also appeared in Fig. 3c and d. There was a peak at 402.3eV in HSVF which was attributed to the protonation of pyridine (Muglali et al. 2011) (Fig. 3d); the strong electrostatic attraction could generate between HSVF and SY, but there was no obvious change in HSF.

Study of adsorption kinetic

Investigation of the kinetic process could provide lots of information about adsorption systems. HSVF and HSF were tested at initial concentrations of 200 mg/L and 100 mg/L respectively. From Fig. 4a and b, HSVF and HSF reached equilibrium at about 12 h and 6 h. The adsorption rates of them exhibited tendencies to go fast and then slow; it could be explained that the adsorption capacity was extreme because of the sufficient adsorption sites and a high concentration gradient at the initial of the adsorption process (Hasan et al. 2023b, 131794; Awual et al. 2023, 124088). Compared to other nonporous adsorbents, their porous

Fig. 3 **a** XPS spectra of HSF and HSVF, **b** N 1s core-level spectra of SY, **c** HSF after adsorption, and **d** HSVF after adsorption
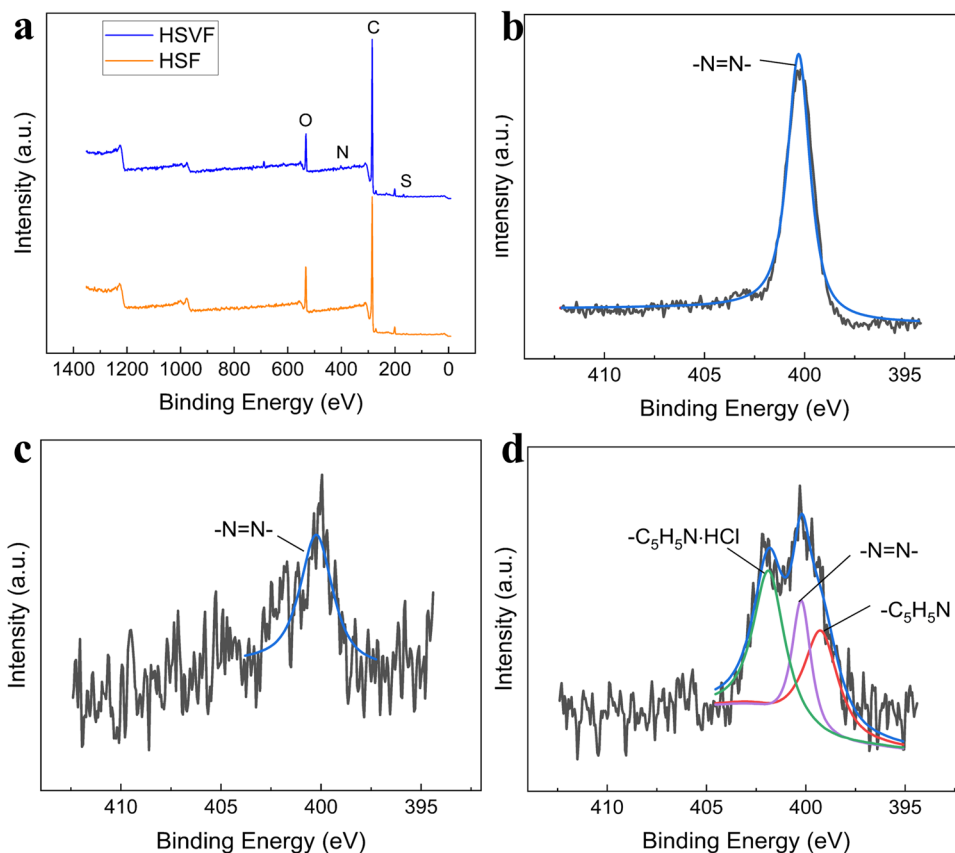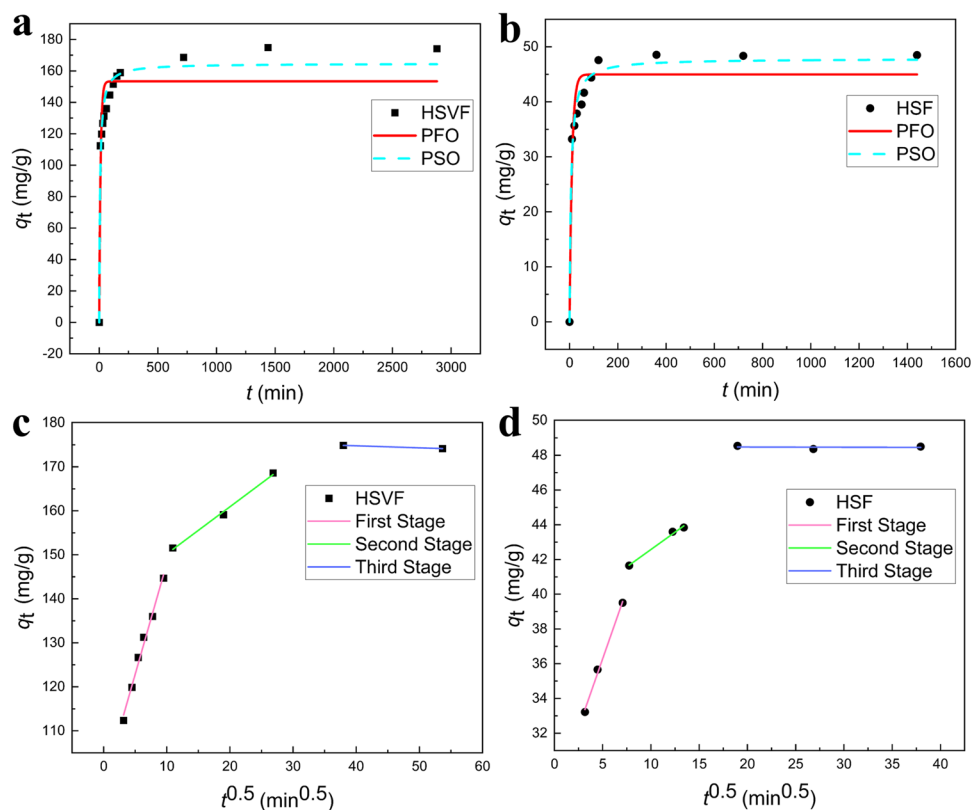
Fig. 4 **a**, **b** Adsorption kinetic curves of HSVF and HSF fitted with PFO (pseudo-first-order-model, red curves) and PSO (pseudo-second-order-model, azure dashed curves), and **c**, **d** intra-particle diffusion model of HSVF and HSF

structure endows them with higher adsorption capacity; thus, their equilibrium time was always longer than nonporous analogues (Tang et al. 2021; Tran et al. 2017). Furthermore, the pseudo-first-order model (PFO) and the pseudo-second-order model (PSO) were used to fit the whole adsorption process and investigate the adsorption mechanism. In general, the adsorption process could be divided into three stages: (1) liquid film diffusion (external diffusion), (2) internal diffusion, and (3) adsorption on active sites. Stage (3) occurred very quickly, so stages (2) and (3) could be regarded as occurring simultaneously (Wang and Guo 2020). The fitting results displayed that PSO was the better model for both of them, which indicated that there was chemisorption for HSVF and HSF during the adsorption processes (Arabkhani and Asfaram 2020).

Generally speaking, as long existed electron transfer or electron pair sharing in the adsorption process, it would be considered chemisorption (Tran et al. 2017). On the one hand, the pyridine structure in HSVF could be protonated and produce strong electrostatic attraction with the sulfonate of the SY molecule, and a hydrogen bond could be formed between the phenolic hydroxy of SY and the pyridine group (Urakawa and Yasue 2019). Besides, π–π stacking could be also generated in the hydrophobic skeleton (Li et al. 2021, 105018). On the other hand, a high chemical potential generated by electrostatic interaction and concentration gradient made diffusion easier, whether external diffusion or internal diffusion.

As for HSF, its aromatic group was electron-rich because of the C-C backbone, and the aromatic group of SY was electron-deficient due to the strong polar group, so the main interaction between SY and HSF was only π–π stacking (Tran et al. 2017). Therefore, the interactions between dyes and HSF were weaker than that between dyes and HSVF.

Furthermore, the intra-particle diffusion model was used to investigate the different stages of adsorption (Fig. 4c and d). The detailed fitting data is listed in Table S1. The whole adsorption process could be divided into three stages. In the first stage, SY molecules diffused through the liquid film; in the second stage, the dye molecules diffused into the pores of the adsorbent and produced the interaction with the active sites at the same time, and in the last stage, the adsorption tended to equilibrium. During the diffusion process, the K_p value of HSVF was always higher than HSF because of the higher chemical potential. Besides, the pore diameter of HSVF was larger than HSF so the influence of sterically hindered effect was reduced during the internal diffusion. However, HSVF needed a longer equilibrium time than HSF because the relatively sufficient adsorption sites needed to be occupied for adsorbate at a higher initial concentration (Chen et al. 2020; Fila et al. 2022, 137245; Zhang et al. 2022, 133604). When decreasing the initial concentration to 100 mg/L for HSVF (Figure S4), its equilibrium time was shorter even though HSF had a higher specific surface area which could provide more contact probability. This could be

explained that HSVF had a higher chemical potential for SY diffusion resulting from the strong electrostatic interaction at the same initial concentration; meanwhile, adsorbates might be more likely to be adsorbed on HSVF due to various interactions. What's more, the weak interaction for HSF might lead to desorption easier because the whole adsorption was a dynamic adsorption-desorption process.

Study of adsorption isotherm

Adsorption isotherm was the relationship between C_e and q_e at a certain temperature. In this study, the isotherms of HSVF and HSF at 298 K, 308 K, and 318 K were investigated, respectively, and Freundlich, Langmuir, and Temkin models were used to fit the isotherm dates, respectively. The detailed fitting dates are listed in Table S2 and Table S3. Generally, both HSVF and HSF preferred to work at low temperature, which illustrated that the adsorption processes were exothermic. As was clearly observed in Fig. 5a, b, and c, the Langmuir model had better fitting results than the other two models for HSVF at each temperature. What's more, the maximal adsorption capacity of the Langmuir model was 343.90 mg/g, which was close to the experimental values (q_e = 331.37 mg/g). This declared that the adsorption on the HSVF was monolayer adsorption, and active sites were distributed uniformly on the surface of HSVF (Hasan et al. 2023b, 131794). Meanwhile, the separation factors of Langmuir model R_L values of each temperature

were between 0 and 1; thereby, this process was a favorable adsorption (Essandoh et al. 2020). Temkin models were suitable for HSF at each temperature and demonstrated that the chemical adsorption positively participated in the adsorption process (Guo et al. 2014, 3081). This result was consistent with the kinetic experiment. In addition, the maximal adsorption capacity of HSVF (331.37 mg/g) was greater than HSF (203.92 mg/g) even though HSF had larger specific surface areas. It could be stated that introducing strong interactions with adsorbates could provide better adsorption performances, because the strong interactions may be favorable for a stable incorporation mechanism between adsorbents and adsorbates (Hasan et al. 2023a, 121125; Salman et al. 2023a, 135259) and improve the adsorption capacity effectively even though high specific surface areas could supply more nanospace (Fu et al. 2022, 8784).

Study of adsorption selectivity

The study of adsorption selectivity for different dye molecules was meaningful for understanding the adsorption mechanism. Therefore, the anionic SY solution was mixed with cationic rhodamine B (RhB) and another anionic methyl blue (MB) for separation testing respectively. In the SY/RhB-mixed dye solution (Fig. 6a), not only the SY dye but also the cationic RhB were removed effectively by HSVF simultaneously. It could be explained that the adsorption of dye molecules by HSVF depends on various interactions.
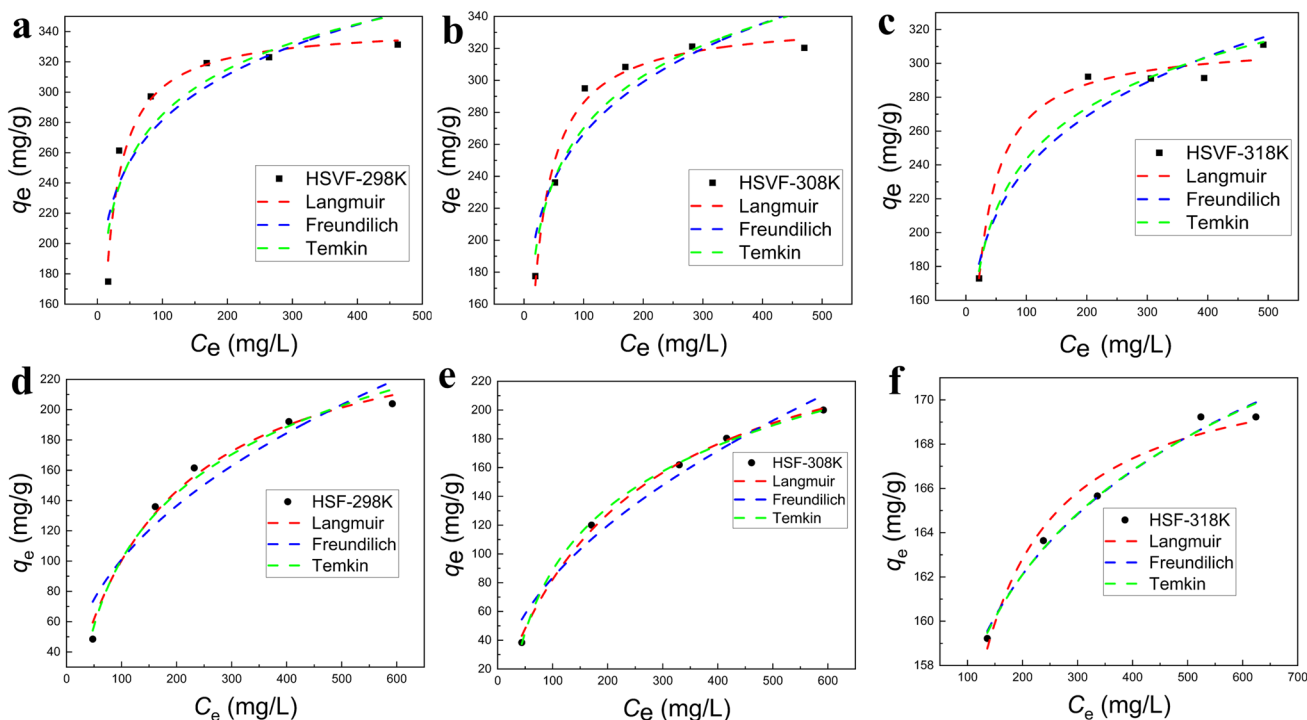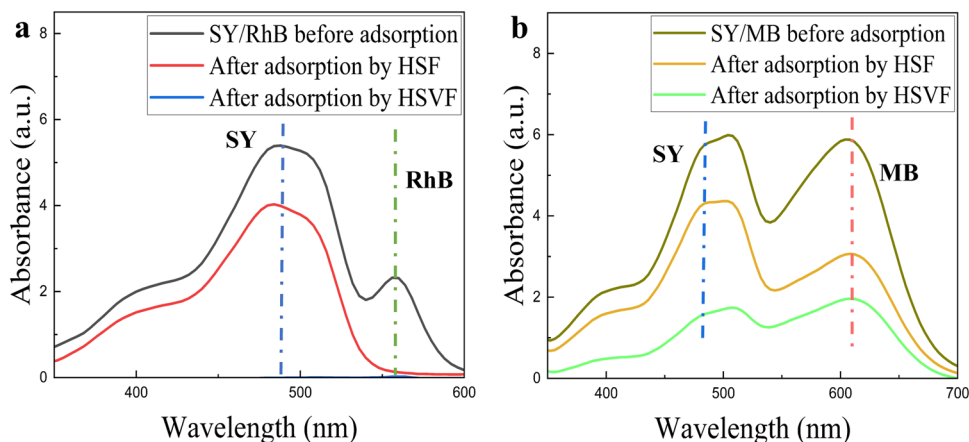

Fig. 5 Isothermal model fitting curves at different temperatures of (a–c) HSVF and (d–f) HSF

Fig. 6 **a** The UV-vis spectra of SY/RhB mixture solution before and after adsorption, **b** the UV-vis spectra of SY/MB mixture solution before and after adsorption

Although there was no electrostatic attraction due to the same charge, the cationic RhB could be adsorbed by π–π stacking and hydrogen bond by HSVF. As for HSF, it could also generate adsorption capacity for anionic and cationic dye in the mixture solution, but the adsorption capacity for RhB was higher than it for SY obviously; the reason might be that the cationic dye molecules tend to aggregate in the protic polar solvents (Sarkar et al. 2008); therefore, the RhB was easy to be adsorbed in abundance. In Fig. 6b, the molecular weight of the dye did not have an obvious influence on adsorption selectivity, the concentrations of SY and MB were decreased, and the adsorption sites were occupied by SY and MB simultaneously. The great adsorption selectivity always came from the unique interactions between adsorbents and adsorbates (Kubra et al. 2023, 131415; Shahat et al. 2015, 286); as for SY and MB, they had similar interactions with adsorbents by sulfonate groups and aromatic rings; therefore, the adsorption selectivity was not obvious. But the adsorption performance of HSVF was better than that of HSF. Therefore, it could be concluded that a nice adsorption performance for both cationic and anionic dye could be realized which relies on various interactions, while more interactions also provided better adsorption capacity.

HSVF could be a promising adsorbent for the multifarious dye wastewater treatment with great potential.

Study of desorption mechanism

The desorption capacity of HSVF and HSF was investigated with 1 M NaOH as a desorption solution. From Fig. 7a, the desorption efficiency of HSVF was increased gradually and tended to balance at last, but the HSF showed an opposite trend. This could be explained that the NaOH solution would change the surface potential of the adsorbent and destroy the interaction between the adsorbent and SY molecules. The strong electrostatic attraction was the dominating interaction between HSVF and SY; it could be influenced greatly by NaOH, so the desorption efficiency of HSVF could reach 85.49% after serval times of desorption. As for HSF, there was no strong electrostatic attraction between HSF and SY. Therefore, less desorption of SY molecules could happen. This result reflected the different electrostatic interactions of HSVF and HSF with SY. What's more, the balance residual adsorption capacities of HSVF and HSF (Fig. 7b) were 5.21 mg/g and 10.76 mg/g respectively; this ratio was in accordance with their pore volume, so it could be inferred that the

Fig. 7 **a** Desorption efficiency of HSVF and HSF, **b** residual adsorption capacity of HSVF and HSF
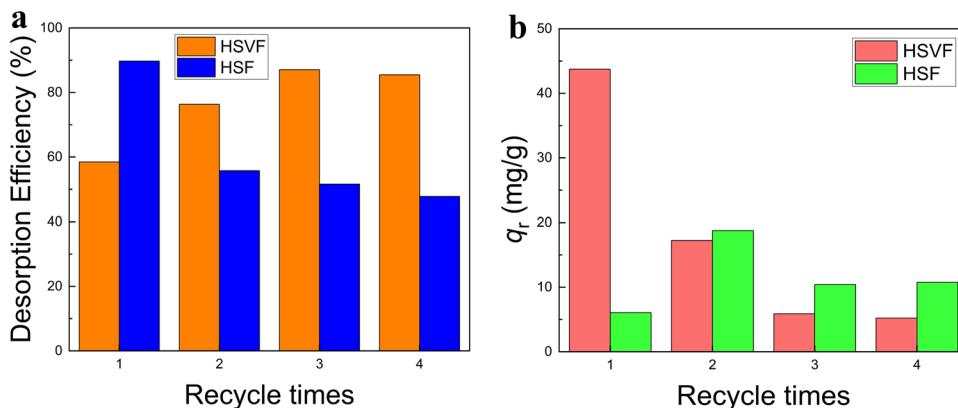
Table 2 Comparison of SY dye maximum adsorption capacity

Adsorbents	q_m (mg/g)	Reference
Mesoporous carbon/neodymium (III) chloride	285.72	(Ahmad et al. 2019, 814)
CaAl-LDH-NO3	398.41	(de Sá et al. 2013, 122)
Polypyrrole/polyaniline nanocomposite	212.1	(Aliabadi and Mahmoodi 2018, 235)
Magnetite nanoparticles/graphene oxide/CTAB	44.25	(Yakout and Mahmoud 2018)
Thermally reduced graphene oxide	243.3	(Coros et al. 2020)
HSF	203.92	This work
HSVF	331.37	

molecules which were hard to be desorbed were anchored in the pore of adsorbent by steric hindrance. HSVF had a nice desorption capacity so that it could be reused easily by combing the magnetism. Besides, it was composed of St, 4VP, and Fe_3O_4, which were all at low cost. So HSVF could be an effective, practical, and economic adsorbent.

Conclusions

In this study, two kinds of magnetic adsorbents HSF and HSVF were synthesized facilely, and their different adsorption behaviors, kinetic, isotherm, selectivity, and desorption behaviors were thoroughly studied. The hybridization with Fe_3O_4 showed a great character of easy operation, which was meaningful to control secondary pollution. In the adsorption experiments, low pH values (pH = 2), low temperature (298 K), and modest solid-to-liquid ratio (1 g/L) were the optimum removal condition. The adsorption experimental result showed nice adsorption capacities for SY (203.92 mg/g and 331.37 mg/g); the comparison with other studies is shown in Table 2. What's more, the adsorption rate and capacity were improved for HSVF compared with HSF because of the existence of stronger active sites even if it has a lower specific surface area. This reflected that the strong interactions between the active sites and dyes played a dominant role during the dye adsorption process. In addition, both HSVF and HSF showed universal adsorption performances for both anionic and cationic dyes, and the unique interaction between adsorbents and adsorbates might be a key factor for great selectivity. Therefore, it could be concluded that introducing strong active sites was an effective method to improve adsorption performances. This research conduces to understand the adsorption process in porous adsorbent system, which could provide some references for the design of future porous adsorbents.

Declarations

References

Ahmad ZU, Yao L, Wang J, Gang DD, Islam F, Lian Q, Zappi ME (2019) Neodymium embedded ordered mesoporous carbon (OMC) for enhanced adsorption of sunset yellow: characterizations, adsorption study and adsorption mechanism. Chem Eng J 359:814–826. https://doi.org/10.1016/j.cej.2018.11.174

Aliabadi RS, Mahmoodi NO (2018) Synthesis and characterization of polypyrrole, polyaniline nanoparticles and their nanocomposite for removal of azo dyes; sunset yellow and Congo red. J Clean Prod 179:235–245. https://doi.org/10.1016/j.jclepro.2018.01.035

Arabkhani P, Asfaram A (2020) Development of a novel three-dimensional magnetic polymer aerogel as an efficient adsorbent for malachite green removal. J Hazard Mater 384:121394. https://doi.org/10.1016/j.jhazmat.2019.121394

Awual MR, Hasan MN, Hasan MM, Salman MS, Sheikh MC, Kubra KT, Islam MS, Marwani HM, Islam A, Khaleque MA, Waliullah RM, Hossain MS, Rasee AI, Rehan AI, Awual ME (2023) Green and robust adsorption and recovery of Europium (III) with a mechanism using hybrid donor conjugate materials. Sep Purif Technol 319:124088. https://doi.org/10.1016/j.seppur.2023.124088

Bolukbasi OS, Yola BB, Boyacioglu H, Yola ML (2022) A novel paraoxon imprinted electrochemical sensor based on MoS(2)NPs@MWCNTs and its application to tap water samples. Food Chem Toxicol 163:112994. https://doi.org/10.1016/j.fct.2022.112994

Castaldo R, Avolio R, Cocca M, Errico ME, Avella M, Gentile G (2021) Amino-functionalized hyper-crosslinked resins for

enhanced adsorption of carbon dioxide and polar dyes. Chem Eng J 418:129463. https://doi.org/10.1016/j.cej.2021.129463

Chen B, Cao Y, Zhao H, Long F, Feng X, Li J, Pan X (2020) A novel Fe(3+)-stabilized magnetic polydopamine composite for enhanced selective adsorption and separation of Methylene blue from complex wastewater. J Hazard Mater 392:122263. https://doi.org/10.1016/j.jhazmat.2020.122263

Cheng B, Le Y, Cai W, Yu J (2011) Synthesis of hierarchical Ni(OH)(2) and NiO nanosheets and their adsorption kinetics and isotherms to Congo red in water. J Hazard Mater 185(2-3):889–897. https://doi.org/10.1016/j.jhazmat.2010.09.104

Cheng XQ, Wang ZX, Jiang X, Li T, Lau CH, Guo Z, Ma J, Shao L (2018) Towards sustainable ultrafast molecular-separation membranes: from conventional polymers to emerging materials. Prog Mater Sci 92:258–283. https://doi.org/10.1016/j.pmatsci.2017.10.006

Coros M, Socaci C, Pruneanu S, Pogacean F, Rosu MC, Turza A, Magerusan L (2020) Thermally reduced graphene oxide as green and easily available adsorbent for Sunset yellow decontamination. Environ Res 182:109047. https://doi.org/10.1016/j.envres.2019.109047

de Sá FP, Cunha BN, Nunes LM (2013) Effect of pH on the adsorption of sunset yellow FCF food dye into a layered double hydroxide (CaAl-LDH-NO3). Chem Eng J 215-216:122–127. https://doi.org/10.1016/j.cej.2012.11.024

El-Safty SA, Shahat A, Awual MR (2011) Efficient adsorbents of nanoporous aluminosilicate monoliths for organic dyes from aqueous solution. J Colloid Interface Sci 359(1):9–18. https://doi.org/10.1016/j.jcis.2011.01.006

Essandoh M, Garcia RA, Gayle MR, Nieman CM (2020) Performance and mechanism of polypeptidylated hemoglobin (Hb)/iron oxide magnetic composites for enhanced dye removal. Chemosphere 247:125897. https://doi.org/10.1016/j.chemosphere.2020.125897

Fila D, Hubicki Z, Kołodyńska D (2022) Applicability of new sustainable and efficient alginate-based composites for critical raw materials recovery: general composites fabrication optimization and adsorption performance evaluation. Chem Eng J 446:137245. https://doi.org/10.1016/j.cej.2022.137245

Fu S-Q, Zhu M-Z, Xue B, Liu P-N (2022) Synergy between ionic capacity and intrinsic porosity in imidazolium-based cationic organic polymers and its effect on anionic dye adsorption. Macromolecules 55(19):8784–8794. https://doi.org/10.1021/acs.macromol.2c01127

Guo H, Chen J, Weng W, Zheng Z, Wang D (2014) Adsorption behavior of Congo red from aqueous solution on La2O3-doped TiO2 nanotubes. J Ind Eng Chem 20(5):3081–3088. https://doi.org/10.1016/j.jiec.2013.11.047

Hasan MM, Kubra KT, Hasan MN, Awual ME, Salman MS, Sheikh MC, Rehan AI, Rasee AI, Waliullah RM, Islam MS, Khandaker S, Islam A, Hossain MS, Alsukaibi AKD, Alshammari HM, Awual MR (2023a) Sustainable ligand-modified based composite material for the selective and effective cadmium(II) capturing from wastewater. J Mol Liq 371:121125. https://doi.org/10.1016/j.molliq.2022.121125

Hasan MM, Salman MS, Hasan MN, Rehan AI, Awual ME, Rasee AI, Waliullah RM, Hossain MS, Kubra KT, Sheikh MC, Khaleque MA, Marwani HM, Islam A, Awual MR (2023b) Facial conjugate adsorbent for sustainable Pb(II) ion monitoring and removal from contaminated water. Colloids Surf A Physicochem Eng Asp 673:131794. https://doi.org/10.1016/j.colsurfa.2023.131794

Hasan MM, Shenashen MA, Hasan MN, Znad H, Salman MS, Awual MR (2021) Natural biodegradable polymeric bioadsorbents for efficient cationic dye encapsulation from wastewater. J Mol Liq 323:114587. https://doi.org/10.1016/j.molliq.2020.114587

Hasan MN, Salman MS, Hasan MM, Kubra KT, Sheikh MC, Rehan AI, Rasee AI, Awual ME, Waliullah RM, Hossain MS, Islam A, Khandaker S, Alsukaibi AKD, Alshammari HM, Awual MR (2023c) Assessing sustainable Lutetium(III) ions adsorption and recovery using novel composite hybrid nanomaterials. J Mol Struct 1276:134795. https://doi.org/10.1016/j.molstruc.2022.134795

Islam A, Teo SH, Taufiq-Yap YH, Ng CH, Vo D-VN, Ibrahim ML, Hasan MM, Khan MAR, Nur ASM, Awual MR (2021) Step towards the sustainable toxic dyes removal and recycling from aqueous solution- a comprehensive review. Resour Conserv Recycl 175:105849. https://doi.org/10.1016/j.resconrec.2021.105849

Jiang X, Huang J (2016) Adsorption of Rhodamine B on two novel polar-modified post-cross-linked resins: equilibrium and kinetics. J Colloid Interface Sci 467:230–238. https://doi.org/10.1016/j.jcis.2016.01.031

Jin L, Wang Y, Xue T, Xie J, Xu Y, Yao Y, Li X (2019) Smart amphiphilic random copolymer-coated sponge with pH-switchable wettability for on-demand oil/water separation. Langmuir 35(45):14473–14480. https://doi.org/10.1021/acs.langmuir.9b02583

Kadirsoy S, Atar N, Yola ML (2020) Molecularly imprinted QCM sensor based on delaminated MXene for chlorpyrifos detection and QCM sensor validation. New J Chem 44(16):6524–6532. https://doi.org/10.1039/d0nj00951b

Karaman C, Karaman O, Yola BB, Ülker İ, Atar N, Yola ML (2021) A novel electrochemical aflatoxin B1 immunosensor based on gold nanoparticle-decorated porous graphene nanoribbon and Ag nanocube-incorporated MoS2 nanosheets. New J Chem 45(25):11222–11233. https://doi.org/10.1039/d1nj02293h

Karaouzas I, Kapetanaki N, Mentzafou A, Kanellopoulos TD, Skoulikidis N (2021) Heavy metal contamination status in Greek surface waters: a review with application and evaluation of pollution indices. Chemosphere 263:128192. https://doi.org/10.1016/j.chemosphere.2020.128192

Kıran TR, Atar N, Yola ML (2019) A methyl parathion recognition method based on carbon nitride incorporated hexagonal boron nitride nanosheets composite including molecularly imprinted polymer. J Electrochem Soc 166(12):H495–H501. https://doi.org/10.1149/2.0331912jes

Kubra KT, Hasan MM, Hasan MN, Salman MS, Khaleque MA, Sheikh MC, Rehan AI, Rasee AI, Waliullah RM, Awual ME, Hossain MS, Alsukaibi AKD, Alshammari HM, Awual MR (2023) The heavy lanthanide of Thulium(III) separation and recovery using specific ligand-based facial composite adsorbent. Colloids Surf A Physicochem Eng Asp 667:131415. https://doi.org/10.1016/j.colsurfa.2023.131415

Kubra KT, Salman MS, Hasan MN (2021a) Enhanced toxic dye removal from wastewater using biodegradable polymeric natural adsorbent. J Mol Liq 328:115468. https://doi.org/10.1016/j.molliq.2021.115468

Kubra KT, Salman MS, Znad H, Hasan MN (2021b) Efficient encapsulation of toxic dye from wastewater using biodegradable polymeric adsorbent. J Mol Liq 329:115541. https://doi.org/10.1016/j.molliq.2021.115541

Li B, Yang X, Xia L, Majeed MI, Tan B (2013) Hollow microporous organic capsules. Sci Rep 3:2128. https://doi.org/10.1038/srep02128

Li F, Cao Y, Hong X, Chen B, Xu M (2021) A facile synthesis of hyper-cross-linked polystyrene resins for phenol removal. React Funct Polym 167:105018. https://doi.org/10.1016/j.reactfunctpolym.2021.105018

Li Q, Jin S, Tan B (2016) Template-mediated synthesis of hollow microporous organic nanorods with tunable aspect ratio. Sci Rep 6:31359. https://doi.org/10.1038/srep31359

Li Q, Zhan Z, Jin S, Tan B (2017) Wettable magnetic hypercrosslinked microporous nanoparticle as an efficient adsorbent for water

treatment. Chem Eng J 326:109–116. https://doi.org/10.1016/j.cej.2017.05.049

Liu JL, Qian WC, Guo JZ, Shen Y, Li B (2021) Selective removal of anionic and cationic dyes by magnetic Fe3O4-loaded amine-modified hydrochar. Bioresour Technol 320(Pt A):124374. https://doi.org/10.1016/j.biortech.2020.124374

Lv C, Chen S, Xie Y, Wei Z, Chen L, Bao J, He C, Zhao W, Sun S, Zhao C (2019) Positively-charged polyethersulfone nanofibrous membranes for bacteria and anionic dyes removal. J Colloid Interface Sci 556:492–502. https://doi.org/10.1016/j.jcis.2019.08.062

Md. Munjur H, Hasan MN, Awual MR, Islam MM, Shenashen MA, Iqbal J (2020) Biodegradable natural carbohydrate polymeric sustainable adsorbents for efficient toxic dye removal from wastewater. J Mol Liq 319:114356. https://doi.org/10.1016/j.molliq.2020.114356

Muglali MI, Bashir A, Terfort A, Rohwerder M (2011) Electrochemical investigations on stability and protonation behavior of pyridine-terminated aromatic self-assembled monolayers. Phys Chem Chem Phys 13(34):15530–15538. https://doi.org/10.1039/c1cp21469a

Nakamura H (2010) Recent organic pollution and its biosensing methods. Anal Methods 2(5):430. https://doi.org/10.1039/b9ay00315k

Naushad M, Alqadami AA, Al-Kahtani AA, Ahamad T, Awual MR, Tatarchuk T (2019) Adsorption of textile dye using para-aminobenzoic acid modified activated carbon: Kinetic and equilibrium studies. J Mol Liq 296:112075. https://doi.org/10.1016/j.molliq.2019.112075

Pavithra KG, Senthil Kumar P, Jaikumar V, Sundar Rajan P (2019) Removal of colorants from wastewater: a review on sources and treatment strategies. J Ind Eng Chem 75:1–19. https://doi.org/10.1016/j.jiec.2019.02.011

Pelin Böke C, Karaman O, Medetalibeyoglu H, Karaman C, Atar N, Lütfi Yola M (2020) A new approach for electrochemical detection of organochlorine compound lindane: development of molecular imprinting polymer with polyoxometalate/carbon nitride nanotubes composite and validation. Microchem J 157:105012. https://doi.org/10.1016/j.microc.2020.105012

Rajendran S, Hoang TKA, Trudeau ML, Jalil AA, Naushad M, Awual MR (2022) Generation of novel n-p-n (CeO(2)-PPy-ZnO) heterojunction for photocatalytic degradation of micro-organic pollutants. Environ Pollut 292(Pt B):118375. https://doi.org/10.1016/j.envpol.2021.118375

Salman MS, Hasan MN, Hasan MM, Kubra KT, Sheikh MC, Rehan AI, Waliullah RM, Rasee AI, Awual ME, Hossain MS, Alsukaibi AKD, Alshammari HM, Awual MR (2023a) Improving copper(II) ion detection and adsorption from wastewater by the ligand-functionalized composite adsorbent. J Mol Struct 1282:135259. https://doi.org/10.1016/j.molstruc.2023.135259

Salman MS, Sheikh MC, Hasan MM, Hasan MN, Kubra KT, Rehan AI, Awual ME, Rasee AI, Waliullah RM, Hossain MS, Khaleque MA, Alsukaibi AKD, Alshammari HM, Awual MR (2023b) Chitosan-coated cotton fiber composite for efficient toxic dye encapsulation from aqueous media. Appl Surf Sci 622:157008. https://doi.org/10.1016/j.apsusc.2023.157008

Sarkar D, Das P, Girigoswami A, Chattopadhyay N (2008) Spectroscopic characterization of phenazinium dye aggregates in water and acetonitrile media: effect of methyl substitution on the aggregation phenomenon. J Phys Chem A 112(40):9684–9691. https://doi.org/10.1021/jp804593v

Shahat A, Awual MR, Khaleque MA, Alam MZ, Naushad M, Chowdhury AMS (2015) Large-pore diameter nano-adsorbent and its application for rapid lead(II) detection and removal from aqueous media. Chem Eng J 273:286–295. https://doi.org/10.1016/j.cej.2015.03.073

Shi P, Chen X, Sun Z, Li C, Xu Z, Jiang X, Jiang B (2020) Thickness controllable hypercrosslinked porous polymer nanofilm with high CO2 capture capacity. J Colloid Interface Sci 563:272–280. https://doi.org/10.1016/j.jcis.2019.12.038

Su P, Zhang X, Xu Z, Zhang G, Shen C, Meng Q (2019) Amino-functionalized hypercrosslinked polymers for highly selective anionic dye removal and CO2/N2 separation. New J Chem 43(44):17267–17274. https://doi.org/10.1039/c9nj02847a

Tang Z, Hu X, Ding H, Li Z, Liang R, Sun G (2021) Villi-like poly(acrylic acid) based hydrogel adsorbent with fast and highly efficient methylene blue removing ability. J Colloid Interface Sci 594:54–63. https://doi.org/10.1016/j.jcis.2021.02.124

Teo SH, Ng CH, Islam A, Abdulkareem-Alsultan G, Joseph CG, Janaun J, Taufiq-Yap YH, Khandaker S, Islam GJ, Znad H, Awual MR (2022) Sustainable toxic dyes removal with advanced materials for clean water production: a comprehensive review. J Clean Prod 332:130039. https://doi.org/10.1016/j.jclepro.2021.130039

Tran HN, You SJ, Hosseini-Bandegharaei A, Chao HP (2017) Mistakes and inconsistencies regarding adsorption of contaminants from aqueous solutions: a critical review. Water Res 120:88–116. https://doi.org/10.1016/j.watres.2017.04.014

Urakawa O, Yasue A (2019) Glass transition behaviors of poly (vinyl pyridine)/poly (vinyl phenol) revisited. Polymers 11(7):1153. https://doi.org/10.3390/polym11071153

Verma AK, Dash RR, Bhunia P (2012) A review on chemical coagulation/flocculation technologies for removal of colour from textile wastewaters. J Environ Manag 93(1):154–168. https://doi.org/10.1016/j.jenvman.2011.09.012

Waheed A, Baig N, Ullah N, Falath W (2021) Removal of hazardous dyes, toxic metal ions and organic pollutants from wastewater by using porous hyper-cross-linked polymeric materials: a review of recent advances. J Environ Manag 287:112360. https://doi.org/10.1016/j.jenvman.2021.112360

Wang J, Guo X (2020) Adsorption kinetic models: physical meanings, applications, and solving methods. J Hazard Mater 390:122156. https://doi.org/10.1016/j.jhazmat.2020.122156

Wu J, Liu J, Wen B, Li Y, Zhou B, Wang Z, Yang S, Zhao R (2021) Nitrogen-rich covalent triazine frameworks for high-efficient removal of anion dyes and the synergistic adsorption of cationic dyes. Chemosphere 272:129622. https://doi.org/10.1016/j.chemosphere.2021.129622

Wu Y, Chen M, Lee HJ, AG M, Zhang N, de Lannoy CF (2022) Nanocomposite polymeric membranes for organic micropollutant removal: a critical review. ACS ES T Eng 2(9):1574–1598. https://doi.org/10.1021/acsestengg.2c00201

Xie G, Lin X, Martinez MR, Wang Z, Lou H, Fu R, Wu D, Matyjaszewski K (2018) Fabrication of porous functional nanonetwork-structured polymers with enhanced adsorption performance from well-defined molecular brush building blocks. Chem Mater 30(23):8624–8629. https://doi.org/10.1021/acs.chemmater.8b03845

Xie H, Du J, Chen J (2020) Concerted efforts are needed to control and mitigate antibiotic pollution in coastal waters of China. Antibiotics 9(2):88. https://doi.org/10.3390/antibiotics9020088

Xu S, Jin Y, Li R, Shan M, Zhang Y (2022) Amidoxime modified polymers of intrinsic microporosity/alginate composite hydrogel beads for efficient adsorption of cationic dyes from aqueous solution. J Colloid Interface Sci 607(Pt 1):890–899. https://doi.org/10.1016/j.jcis.2021.08.157

Yadav S, Asthana A, Singh AK, Chakraborty R, Vidya SS, Susan M, Carabineiro SAC (2021) Adsorption of cationic dyes, drugs and metal from aqueous solutions using a polymer composite of magnetic/beta-cyclodextrin/activated charcoal/Na alginate: isotherm, kinetics and regeneration studies. J Hazard Mater 409:124840. https://doi.org/10.1016/j.jhazmat.2020.124840

Yakout AA, Mahmoud ME (2018) Fabrication of magnetite-functionalized-graphene oxide and hexadecyltrimethyl ammonium bromide nanocomposite for efficient nanosorption of sunset yellow. Mater

Sci Eng C Mater Biol Appl 92:287–296. https://doi.org/10.1016/j.msec.2018.06.060

Yeamin MB, Islam MM, Chowdhury A-N, Awual MR (2021) Efficient encapsulation of toxic dyes from wastewater using several biodegradable natural polymers and their composites. J Clean Prod 291:125920. https://doi.org/10.1016/j.jclepro.2021.125920

Yola ML (2022) Carbendazim imprinted electrochemical sensor based on CdMoO(4)/g-C(3)N(4) nanocomposite: application to fruit juice samples. Chemosphere 301:134766. https://doi.org/10.1016/j.chemosphere.2022.134766

Zhang H, Li M, Liu Z, Zhang X, Du C (2022) Two Keggin-type polyoxometalates used as adsorbents with high efficiency and selectivity toward antibiotics and heavy metals. J Mol Struct 1267:133604. https://doi.org/10.1016/j.molstruc.2022.133604

Zhang L, Xin Z, Fei X, Luo H, Li H, Lu B, Li Z, Wei G (2019) Study on adsorption of tetracycline by red mud-based ceramsite. J Water Supply Res Technol AQUA 68(1):39–50. https://doi.org/10.2166/aqua.2018.100

Zhang M, Zhou Q, Li A, Shuang C, Wang W, Wang M (2013) A magnetic sorbent for the efficient and rapid extraction of organic micropollutants from large-volume environmental water samples. J Chromatogr A 1316:44–52. https://doi.org/10.1016/j.chroma.2013.09.086

Zhang Y, Hong X, Cao XM, Huang XQ, Hu B, Ding SY, Lin H (2021) Functional porous organic polymers with conjugated triaryl triazine as the core for superfast adsorption removal of organic dyes. ACS Appl Mater Interfaces 13(5):6359–6366. https://doi.org/10.1021/acsami.0c21374

Zhang Z, Rahman MM, Abetz C, Hohme AL, Sperling E, Abetz V (2020) Chemically tailored multifunctional asymmetric isoporous triblock terpolymer membranes for selective transport. Adv Mater 32(8):e1907014. https://doi.org/10.1002/adma.201907014

Zhao W, Jiao Y, Gao R, Wu L, Cheng S, Zhuang Q, Xie A, Dong W (2020) Sulfonate-grafted conjugated microporous polymers for fast removal of cationic dyes from water. Chem Eng J 391:123591. https://doi.org/10.1016/j.cej.2019.123591

Zhou M, Wang T, He Z, Xu Y, Yu W, Shi B, Huang K (2019) Synthesis of yolk–shell magnetic porous organic nanospheres for efficient removal of methylene blue from water. ACS Sustain Chem Eng 7(3):2924–2932. https://doi.org/10.1021/acssuschemeng.8b01807

Zhu R, Chen Q, Zhou Q, Xi Y, Zhu J, He H (2016) Adsorbents based on montmorillonite for contaminant removal from water: a review. Appl Clay Sci 123:239–258. https://doi.org/10.1016/j.clay.2015.12.024

Zou W, Bai H, Gao S, Li K (2013) Characterization of modified sawdust, kinetic and equilibrium study about methylene blue adsorption in batch mode. Korean J Chem Eng 30(1):111–122. https://doi.org/10.1007/s11814-012-0096-y